Aerosol Science and Technology

ISSN: 0278-6826 (Print) 1521-7388 (Online) Journal homepage: http://www.tandfonline.com/loi/uast20

Mathematical Description of Experimentally Determined Charge Distributions of a Unipolar Diffusion Charger

Heinz Kaminski , Thomas A. J. Kuhlbusch , Heinz Fissan , Lavanya Ravi , Hans-Georg Horn , Hee-Siew Han , Rob Caldow & Christof Asbach

To cite this article: Heinz Kaminski , Thomas A. J. Kuhlbusch , Heinz Fissan , Lavanya Ravi , Hans-Georg Horn , Hee-Siew Han , Rob Caldow & Christof Asbach (2012) Mathematical Description of Experimentally Determined Charge Distributions of a Unipolar Diffusion Charger, Aerosol Science and Technology, 46:6, 708-716, DOI: 10.1080/02786826.2012.659360

To link to this article: http://dx.doi.org/10.1080/02786826.2012.659360

Accepted online: 23 Jan 2012.

Aerosol Science and Technology, 46:708–716, 2012

ISSN: 0278-6826 print / 1521-7388 online
DOI: 10.1080/02786826.2012.659360

Mathematical Description of Experimentally Determined Charge Distributions of a Unipolar Diffusion Charger

Heinz Kaminski,[1] Thomas A. J. Kuhlbusch,[1,2] Heinz Fissan,[1,2] Lavanya Ravi,[1] Hans-Georg Horn,[3] Hee-Siew Han,[4] Rob Caldow,[4] and Christof Asbach[1]

[1]*Air Quality & Sustainable Nanotechnology Unit, Institute of Energy and Environmental Technology (IUTA) e.V., Duisburg, Germany*
[2]*Center for NanoIntegration Duisburg-Essen (CeNIDE), Duisburg, Germany*
[3]*TSI GmbH, Aachen, Germany*
[4]*TSI Inc., Shoreview, Minnesota, USA*

The charge distributions of an improved opposed flow unipolar diffusion charger were measured using a tandem differential mobility analyzer (DMA) set up in a size range of approximately 20–400 nm. The charger is intended to be used in a portable aerosol sizer to measure particle size distributions. The determined charge distributions were represented by lognormal distributions, and a set of equations and coefficients was developed to calculate the charge distributions. These equations can be easily implemented in software for size distribution measurements. The agreement between the mathematically derived and measured charge distributions is very good, with regression coefficients $R^2 > 0.96$. The investigations showed that approximately 55% of 20-nm particles remain uncharged, while up to 25 elementary charges need to be considered for multiple charge correction of 400-nm particles. Comparison with the Fuchs theory delivered satisfying agreement with the measured average charge levels, but charge distributions cannot be described by the Fuchs theory, likely caused by the charger geometry.

INTRODUCTION

Engineered nanomaterials have been reported to be of possible health concern (Oberdörster 2000; Hoet et al. 2004; Nel et al. 2006; Poland et al. 2008). The highest possibility for exposure to engineered nanoparticles (the term "nanoparticle" is here synonymously also used for nanoplates and nanofibers) exists in occupational settings, where such particles are produced, handled, or used otherwise (Schulte et al. 2008). Studies on the possible exposure to engineered nanoparticles in work environments have therefore raised increased attention in the past. Since inhalation is seen as the major uptake route, exposure to airborne nanoparticles needs to be assessed, e.g., in view of worker protection. The best estimate of a worker's exposure can be derived from mobile, ideally personal measurements, taking aerosol samples in the breathing zone of the worker. Personal samplers for nanoparticles, however, are currently all more or less still at a research level (Azong-Wara et al. 2009; Furuuchi et al. 2010; Cena et al. 2011). Due to the lack of suitable personal measurement equipment, extensive measurement campaigns with a large set of bulky equipment are commonly carried out for a detailed assessment of possible exposure. Reviews of nanoparticle exposure measurements in industrial settings have recently been published by Brouwer et al. (2009) and Kuhlbusch et al. (2011). Those campaigns usually require extensive equipment and their data evaluation can be very time-consuming. Methner et al. (Methner, Hodson, and Geraci 2010; Methner, Hodson, Dames et al. 2010) and the German Chemical Industry Association (VCI 2011) recently published a tiered approach to assess possible exposure. The first tier foresees a rough assessment of the particle concentration by means of portable measurement devices. Requirements for such mobile nanoparticle exposure monitors are small size, low weight and power consumption. The discussion on the health relevance of different aerosol metrics, to be determined by such monitors, is still ongoing (Maynard and Aitken 2007; Oberdörster et al. 2007; Wittmaack 2007), and hence, a sophisticated exposure monitor should provide versatile information on the aerosol, i.e., the particle size distribution which under several assumptions can also be converted into size integrated number, surface area, or volume/mass concentrations. Besides the abovementioned requirements, a portable or personal workplace monitor must not use any harmful substances. Bipolar aerosol chargers using

Received 2 September 2011; accepted 26 December 2011.
The research leading to these results has received funding from the European Community's Seventh Framework Programme (FP7/2007-2013) under grant agreement no. 211464-2.
Address correspondence to Christof Asbach, Air Quality & Sustainable Nanotechnology Unit, Institute of Energy and Environmental Technology (IUTA) e.V., 47229 Duisburg, Germany. E-mail: asbach@iuta.de

radioactive materials, as commonly used in electrical mobility particle sizers, should hence not be used. Unipolar diffusion chargers, based on electrical corona discharge, are therefore a preferred option. Unipolar diffusion chargers exist in a large variety of designs and some of them were explicitly developed for miniaturized nanoparticle measurement devices (Qi et al. 2008; Park et al. 2010). Commercial, portable devices that are based on unipolar diffusion charging to determine nanoparticle concentrations include the *NanoCheck* (Grimm Aerosoltechnik) and the *NanoTracer* (Philips Aerasense; Marra et al. 2010), which both determine number concentration and mean particle size based on the assumption of unimodal lognormal size distributions. Further devices are the *Aerotrak 9000* (TSI Inc.), which determines lung-deposited surface area concentration, and the *miniDiSC* (FH Nordwestschweiz; Fierz et al. 2011, meanwhile commercialized as DiSCmini by Matter Aerosol), which measures number concentration, lung-deposited surface area concentration, and mean particle size. None of the devices, however, measures particle size-resolved concentrations, which would allow for a more detailed analysis of the workplace aerosol.

Unipolar diffusion chargers provide higher charge levels than bipolar chargers, which at the same time can be advantageous and disadvantageous. If the concentration is determined by electrical means, i.e., with an electrometer, the higher charge level provides a better signal and therefore allows for the measurement of lower concentrations. This is an advantage of devices for integrated concentration measurements. On the other hand, the charge and hence mobility distribution for each particle size are broader, making multiple charge correction (MCC; Hoppel 1978) in the data deconvolution algorithm of size distribution measurements more complex. To perform the MCC procedure correctly, the charge distribution has to be well known and mathematically described in a way that can be implemented in a software algorithm. We here present work on the experimental evaluation and mathematical description of a unipolar diffusion charger, which is intended to be used in a portable aerosol sizer, which will allow for the measurement of particle size distributions. In the aerosol sizer, large particles are first removed in a combination of virtual impactor and cyclone (Asbach et al. 2011). The remaining particles are then unipolarly charged, mobility-classified, and the concentration of the classified aerosol is eventually electrically measured. The aerosol sizer is intended to measure up to an electrical mobility-equivalent particle diameter of 400 nm, thus up to the minimum of the particle lung deposition curve. The size range hence covers nanoparticles and their smaller agglomerates. Extending the size range for electrical mobility analysis of unipolarly charged particles above this range is usually not easily possible, because the Cunningham slip correction factor approaches unity. With a charging efficiency of the unipolar diffusion charger being approximately proportional to particle diameter, the electrical mobility of particles larger than approximately 400 nm becomes almost independent of particle size. Electrical mobility analysis therefore loses its particle size resolution. From previous investigations using the unipolar diffusion charger from a nanoparticle surface area monitor (NSAM; TSI, model 3550), the lower detection limit is expected to be at approximately 20 nm (Asbach et al. 2009), depending on the concentration.

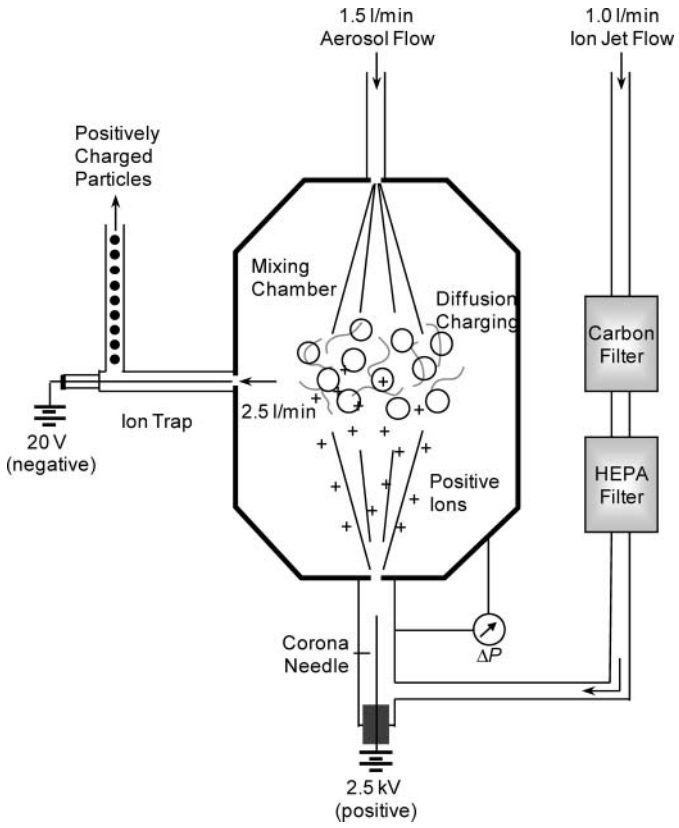

FIG. 1. Schematic of opposed flow diffusion charger.

Charger Design

The unipolar charger under investigation uses the opposed flow principle as introduced by Medved et al. (2000), which is depicted in Figure 1. The total inlet flow of 2.5 l min^{-1} is split into a 1.5-l min^{-1} aerosol flow and a 1-l min^{-1} ion jet flow, which is completely filtered and passes a corona needle to convectively transport ions into a mixing chamber, where the ion flow mixes with the aerosol flow. Due to the absence of any electric fields inside the mixing chamber, ions attach to the particles by pure diffusion. Downstream of the mixing chamber, ions are removed in an ion trap, which consists of a concentric set-up with inner and outer electrodes. A low voltage (20 V) is applied to the inner electrode to remove the ions. A small fraction of especially highly mobile particles is also removed from the aerosol flow, thus affecting the extrinsic charging efficiency.

This type of charger is used in commercial devices, such as the NSAM (TSI model 3550; Fissan et al. 2007; Shin et al. 2007), electrical aerosol detector (EAD; TSI model 3070A), or the ultrafine particle monitor (UFP monitor; TSI model 3031).

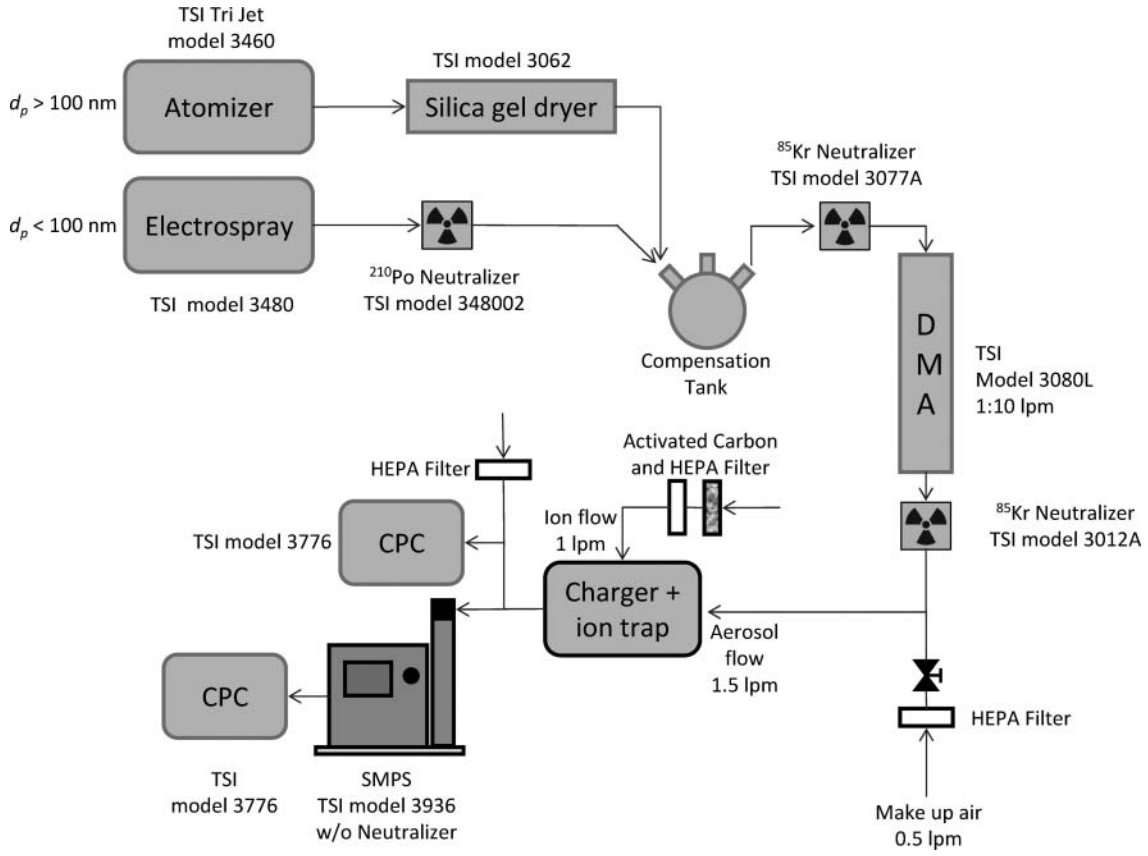

FIG. 2. Experimental set-up to measure particle charge distribution.

Li et al. (2009) used the EAD also for size distribution measurements, based on average charge levels. Jung and Kittelson (2005) found that at least in a size range of 30–150 nm, the average charge level can be approximated by the particle diameter to a power of 1.13. In a previous publication (Asbach et al. 2009), we showed that NSAM can only deliver accurate results in a size range of 20–400 nm, where the charger delivers a charge level that can be exploited in the NSAM to measure surface area concentrations that would deposit in different regions of the human respiratory system, which all follow approximately the same particle size dependence. Qi et al. (2009) showed that the average charge levels of initially neutral particles agree well with Fuchs' theory (1963), in combination with birth-and-death theory proposed by Boisdron and Brock (1970), if a product of ion concentration and residence time (*nt* product) of 2.5×10^{13} s m^{-3} is assumed. The charger principle is well proven, but difficulties with the cleaning procedure of the corona needle were reported to the manufacturer. As a result, the charger design was re-evaluated in order to assure easier cleaning. In the earlier version of the charger, the corona needle consisted of a short piece of a platinum wire of 100-μm diameter that could bend during the cleaning process and bias the charging efficiency. The wire was furthermore not easily accessible. The wire was now replaced by a rigid, sharp needle made of 90% platinum and 10% iridium that is directly connected to a plastic knob that can easily be screwed in and out of the charger housing. The same knob is used to install the inner electrode of the ion trap.

EXPERIMENTAL

The particle charge distributions were measured with monodisperse particles between 19 and 399 nm in size using a typical tandem differential mobility analyzer (DMA) set-up (Qi et al. 2008) shown in Figure 2. Di-ethyl-hexyl-sebacate (DEHS, $C_{26}H_{50}O_4$) particles of diameters 19, 31, 51, 73, and 99 nm were produced with an electrospray (TSI model 3480; Chen et al. 1995). The electrospray system is equipped with a ^{210}Po neutralizer (TSI model 348002) to immediately neutralize the particles in order to avoid extensive electrostatic particle losses. Particle diameters are based on DMA sizing. DEHS was diluted with different amounts of a buffer solution to obtain the aforementioned particles sizes. The buffer solution contained 67-mM ammonium acetate ($C_2H_7NO_2$) created by dissolving ammonium acetate in a 50:50 mix of isopropyl alcohol and ethanol. PSL particles of diameters 131, 182, 246, 305, 356, and 399 nm were generated from aqueous PSL suspensions with a Tri Jet atomizer (TSI model 3460) and dried with a silica

gel diffusion dryer (TSI model 3062). Since the flow rates of the aerosol generators did not match the DMA aerosol flow, a compensation tank with an open vent was used, before particles were brought to charge equilibrium in an ^{85}Kr neutralizer (TSI model 3077A) and size-classified in a DMA (TSI long model 3080L) to obtain monodisperse particles. Up to a particle size of 246 nm, the DMA was operated at 1-l min^{-1} aerosol flow and 10-l min^{-1} sheath flow and voltages corresponding with the mobility of singly charged particles of the produced particle sizes. To adjust the DMA size range to the required particle sizes, the flow rates were changed to 0.7 l min^{-1} aerosol flow and 7 l min^{-1} sheath flow for particles sizes of 305 nm and 356 nm, and 0.6 l min^{-1} aerosol flow and 6 l min^{-1} sheath flow for 399-nm particles. Downstream of the DMA, particles were neutralized again with another ^{85}Kr neutralizer (TSI model 3012A), because Qi et al. (2009) showed that pre-existing charges can bias the charging efficiency of a unipolar charger if charger and pre-existing charge have the same polarity. Neutralized particles were chosen for the charger characterization instead of the often-used uncharged particles, because it represents the commonly seen charge distribution of airborne particles. Certainly, the eventual charge distributions may differ in real measurements from the ones determined here if the airborne charge distributions are significantly different from equilibrium. However, as Qi et al. (2009) have shown, for the positive diffusion charger used here, this only applies to positively pre-charged aerosols. A possible solution would be the use of a first charger with negative polarity upstream of the positive charger, as used, e.g., in the fast mobility particle sizer (FMPS, TSI model 3091). In the experiments, the monodisperse, neutralized aerosol was introduced into the charger and ion trap unit, which was operated at 1.5-l min^{-1} aerosol flow and 1-l min^{-1} ion jet flow.

The corona current was kept constant at 1 μA, corresponding to a corona voltage of approximately 2.1 kV, and the ion trap voltage was set to 20 V. Downstream of the charger and ion trap unit, a second identical DMA, incorporated into the SMPS (TSI model 3936), was used without neutralizer to measure the mobility distribution of the charged particles with DMA flow rates of 1.5-l min^{-1} aerosol flow and 16.5 l min^{-1} sheath flow. The raw mobility distribution was obtained by switching off the MCC of the SMPS software (TSI Aerosol Instrument Manager Software, Release Version 8.1.0.0). Since in that case the software reports the concentration in each size channel assuming a single particle charge, the obtained concentration data were multiplied with the probability of singly charged particles. Since the size of the particles is known from the DMA classification, the mobility distribution can directly be related to particle charge distribution.

RESULTS AND DISCUSSION

The measured mobility distribution is exemplarily shown for 131-nm particles in Figure 3. The distributions for each number of elementary charges were mathematically fitted to lognormal

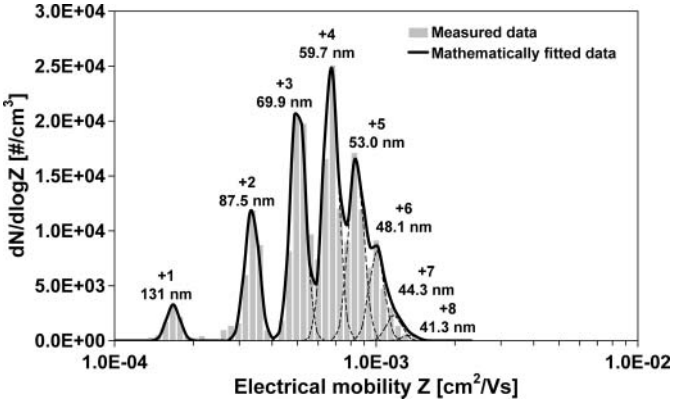

FIG. 3. Mobility distribution of 131-nm PSL particles (DMA flow rates: 1.5 l min^{-1} aerosol, 16.5 l min^{-1} sheath air).

distributions (dotted line in Figure 3) and the single distributions summed up (straight line in Figure 3). The agreement between the fitted and the measured mobility distributions are very good, with regression coefficients in the range of $0.971 \leq R^2 \leq 0.998$. The different charge fractions always followed a lognormal distribution so that they could be mathematically fitted and differentiated, even if the distributions were overlapping, as, e.g., in the case of 6–8 elementary charges shown in Figure 3. The total number concentrations of the monodisperse test particles were in a range of 2700–13,800 particles cm^{-3} . In addition, the fraction of uncharged particles was determined by measuring the number concentration in the DMA sheath flow, with the DMA operating at –10,000 V, so that all charged particles within the considered electrical mobility range were removed in the DMA. To do so, the condensation particle counter (CPC) of the SMPS was directly connected to the sheath flow path. During all measurements, a second CPC measured the total number concentration in parallel to the SMPS. As a quality control measure, the sum of the different charge fractions was eventually compared with the total concentration but differences were found to be less than 1%, i.e., negligible.

The percentages of the different charge fractions were determined for each particle size d_p by integrating the fitted lognormal distributions for each individual charge fraction n. The ratio of the concentration of this charge fraction n and the total concentration is the probability of a particle of the given size to acquire n elementary charges in the unipolar diffusion charger. The charge distributions of the 11 investigated particle sizes between 19 and 399 nm showed that the fraction of uncharged particles is negligible above approximately 100 nm and approximately 55% for 19-nm particles. For 399-nm particles, charge levels of up to 25 elementary charges need to be considered. The average charge level as a function of particle size was calculated from the charge distributions and is shown in Figure 4 (triangles), together with results from the NSAM charger, measured by Jung and Kittelson (2005) (line) and us (Asbach et al. 2011) (circles). The exponent of the fit to the charge levels was 1.13 with the NSAM charger and is 1.12 with the present

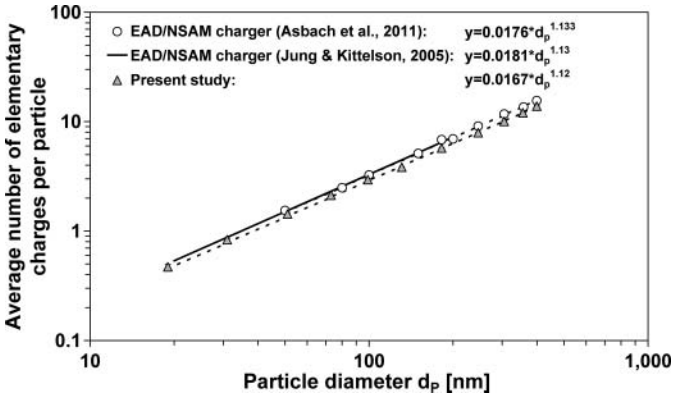

FIG. 4. Mean charge per particle in comparison with EAD/NSAM version (Jung and Kittelson 2005; Asbach et al. 2011).

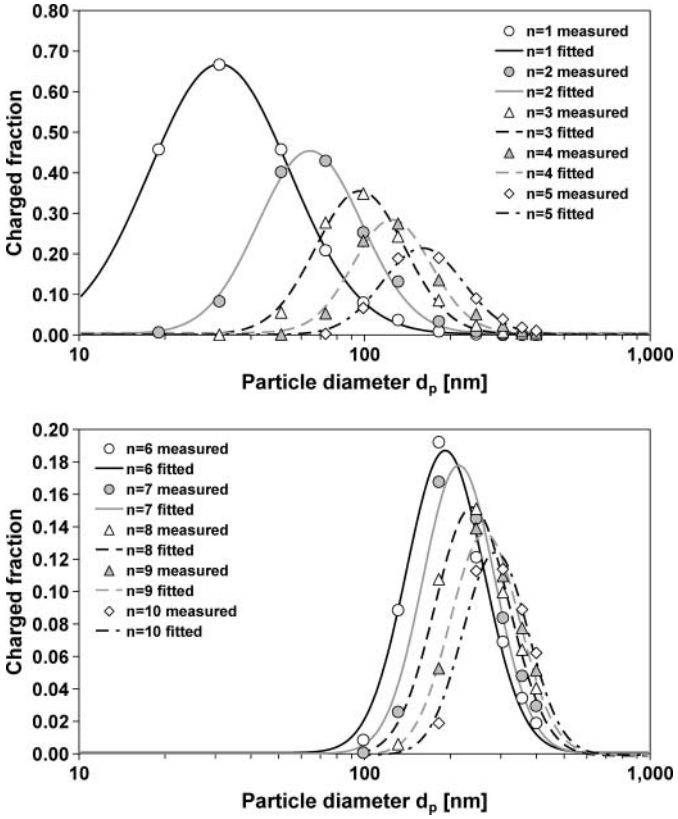

FIG. 5. Measured (symbols) and fitted (lines) data for the charged fraction as a function of particle size for 1–5 (top) and 6–10 (bottom) elementary charges.

one; hence, almost identical. This shows that due to the very comparable charging efficiency, the new charger design is also suitable for the estimation of particle length concentrations, as in the EAD (TSI model 3070A), and to measure lung-deposited surface area concentrations, as in the NSAM (TSI model 3550). The slightly different coefficients, 0.0167 with the new charger compared with 0.0181, would only require an adjustment of the calibration factor of the respective device but do not affect the instrument response as a function of particle size.

In order to be able to use the unipolar charger in electrical mobility analysis for the determination of particle size distributions, the charge distribution needs to be mathematically described with equations that can be implemented in data evaluation software. Similar to the numerical approximation of the charge distribution by Wiedensohler (1988), the probability η_n of a particle to acquire n elementary charges needs to be expressed as a function of particle size d_p. In Figure 5, the measured charge distributions are shown as symbols for singly to five-fold charged particles (top) and six- to ten-fold charged particles (bottom). The distributions of these charge fractions follow lognormal distributions so that they could be mathematically fitted to the following equation, using the statistics software package IGOR (Pro version 6.0, WaveMetrics, Inc.):

$$\eta_n(d_\mathrm{p}) = y_0(n) + A(n) \cdot \exp\left\{-\left(\frac{\ln(d_\mathrm{p}) - \ln(CMD(n))}{B(n)}\right)^2\right\}. \quad [1]$$

In Equation (1), $y_0(n)$ describes a possible vertical shift, $A(n)$ is a coefficient describing the overall probability of a particle to acquire n elementary charges, d_p is the particle diameter, $CMD(n)$ is the count median diameter of the lognormal distribution for n elementary charges, and $B(n)$ is a coefficient determining the width, i.e., the geometric standard deviation of the distribution. Although only shown up to $n = 10$ in Figure 5, fitting was carried out up to 15 elementary charges. Fitting of the distributions for charge levels $n > 15$ was not meaningful, because within the measured particle size range, charge distributions only covered a part of the left branch, i.e., increasing branch of the lognormal distribution, but not the right branch. The graphs show that the fitting works very well for up to five elementary charges, whereas the quality of the fit gets somewhat worse for higher numbers, mainly due to the decreasing number of experimental data points. However, the contribution of the higher charge levels gets increasingly lower and hence possible inaccuracies of the fitting only have a minor impact on the eventual size distribution calculation.

The fit data are summarized in Table 1. The vertical shift y_0 is expectedly close to zero for all charged fractions, except for $n = 0$ and $n = 15$. In these cases, the fits were generally bad and none of the fitted parameters was further used. For all other cases ($1 \leq n \leq 14$), y_0 was set to zero in the following. The values in the table clearly show that the fitting procedure fails for the uncharged fraction and for 15 and more elementary charges, whereas it does work well for lower numbers. Hence, fit data from charge levels $1 \leq n \leq 14$ were further processed to develop a set of equations that can be extrapolated also for higher charge levels. As shown in Figure 6, all parameters of Equation (1), listed in Table 1, could be mathematically fitted

TABLE 1
Coefficients of lognormal charge distributions

n	$y_0(n)$	$A(n)$	$CMD(n)$	$B(n)$
0	14.926	14.962	177.72	11.816
1	0.00207591	0.665802	31.0616	0.796972
2	0.0035097	0.45047	64.38	0.58971
3	0.0026258	0.35273	96.496	0.50573
4	0.0055639	0.27899	124.7	0.44314
5	0.0012087	0.21304	159.79	0.46192
6	0.00065724	0.18632	191.64	0.43956
7	0.00021328	0.1776	213.99	0.41053
8	−0.0011655	0.15337	238.1	0.42165
9	−0.00066695	0.13683	263.98	0.39516
10	−0.00068035	0.12513	287.51	0.37299
11	−0.00066212	0.011781	310.05	0.34887
12	−0.00031997	0.11195	330.29	0.31633
13	−0.00024211	0.10693	347.87	0.28299
14	−0.00027853	0.098539	369.46	0.27563
15	1.8336	−1.8471	56.255	9.0672

to the following empirical general equation:

$$f_x(n) = K_a + K_b \cdot e^{-K_c \cdot i} + K_d \cdot e^{-K_e \cdot i} \begin{cases} f_x \in \{A, B, CMD\} \\ i = 0.412 \text{ for } n = 0 \\ i = n \text{ for } n \geq 1, n \in N \end{cases}, \quad [2]$$

where $f_x(n)$ stands for the three parameters $A(n)$, $CMD(n)$, and $B(n)$; K_a through K_e are coefficients from the fitting; and i is a running index. The running index i is equal to the number n of elementary charges for $n \geq 1$. As Figure 6 shows, the fitting works very well for the three parameters, with regression coefficients R^2 of 0.9983 (A), 0.9805 (B), and 0.9997 (CMD), respectively. The values of the coefficients K_a through K_e for the parameters A, B, and CMD for $n \geq 1$ are given in Table 2. The data in Table 1 show that the case of uncharged particles ($n = 0$) needed a different approach.

However, it was found that Equation (2) can also be used for this case if i is set to 0.412. The data in Table 2 were determined only from charge fractions $1 \leq n \leq 14$, but can be used for higher charge levels using Equations (1) and (2), as shown in Figure 7, for all charge levels $0 \leq n \leq 25$. The comparison of measured (shown as symbols in Figure 7) and calculated (represented as lines) charge fractions show very good agreement. Table 3 gives the regression coefficients of calculated and measured charge fractions—those could only be calculated for charge levels between 0 and 14 elementary charges, because the number of experimental data points was not sufficient for higher charge levels. Regression coefficients (R^2) between 0.973 and 0.999, however, prove the high quality of the set of equations for estimating the charge distributions. Equations (1) and (2), along with the empirical coefficients in Table 2, can be easily implemented in data acquisition and evaluation software to calculate the size-dependent charge fractions as needed for size distribution measurements.

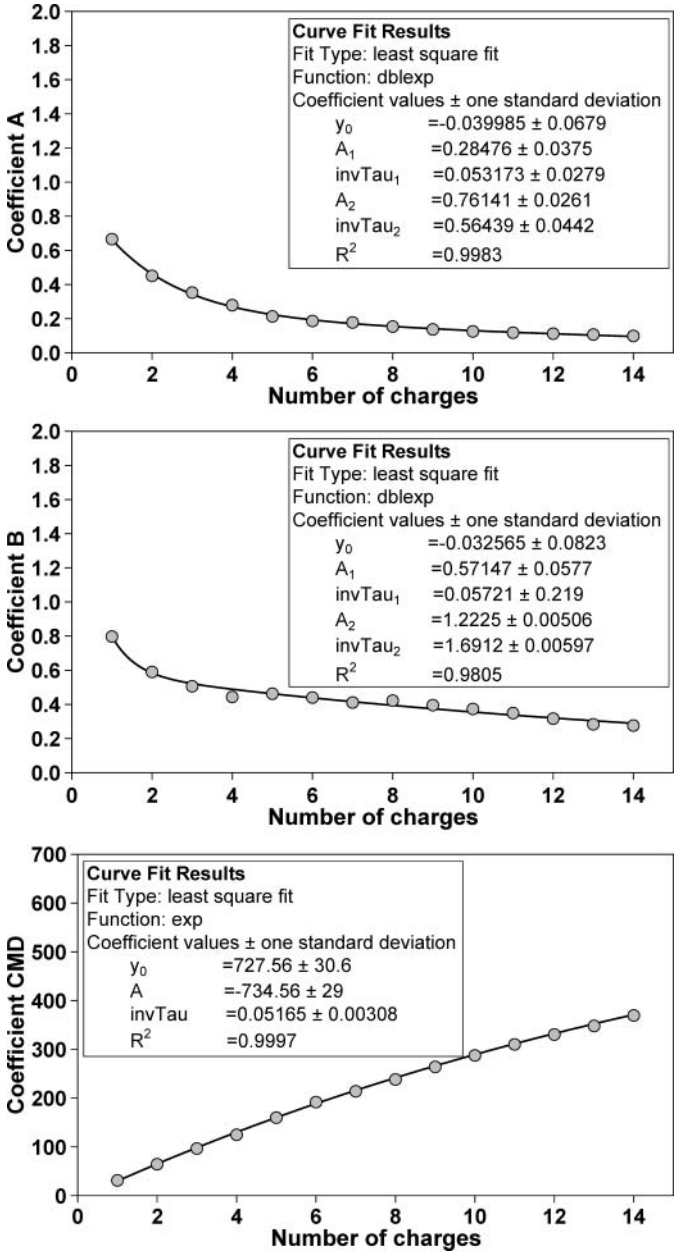

FIG. 6. Fitting of parameters of lognormal distributions.

Eventually, the charge distributions calculated from Equations (1) and (2) were compared with charge distributions obtained from Fuchs' model (1963), assuming ion mobility and mass of 1.15×10^{-4} m^2 V^{-1} m^{-1} and 0.29 kg mol^{-1}, respectively (taken from Qi et al. 2009). The calculations were based on the common assumption that the ion concentration is much higher than the particle concentration. Best comparability of results was obtained for an nt product of ion concentration and particle residence time of 7×10^{12} s m^{-3}, which is lower than the nt product of 2.5×10^{13} s m^{-3} determined by Qi et al.

TABLE 2
Empirical coefficients for Equation (2)

	Coefficients				
	K_a	K_b	K_c	K_d	K_e
A	−0.039985	0.28476	0.053173	0.76141	0.56439
CMD	727.56	−734.56	0.05165	0	0
B	0.032565	0.57147	0.05721	1.225	1.6912

TABLE 3
Regression coefficients of calculated (Equations 1 and 2) and measured charge fractions

n	0	1	2	3	4	5	6	7	8	9	10	11	12	13	14
i	0.412	1	2	3	4	5	6	7	8	9	10	11	12	13	14
R^2	0.9995	0.9970	0.9944	0.9925	0.9726	0.9913	0.9834	0.9734	0.9828	0.9892	0.9890	0.9962	0.9980	0.9963	0.9981

(2009) for the NSAM charger. Differences in the ion concentration are likely caused by the different corona needle design used in the present charger. The lower ion concentration is reflected in the somewhat lower charging efficiency of the new charger (Figure 4). The calculated charge distributions are shown for $1 \leq n \leq 8$, along with the ones calculated from Equations (1) and (2), in Figure 8. All charge distributions calculated according to Fuchs' model follow a lognormal distribution, thus justifying the assumption of lognormal distributions for Equation (1).

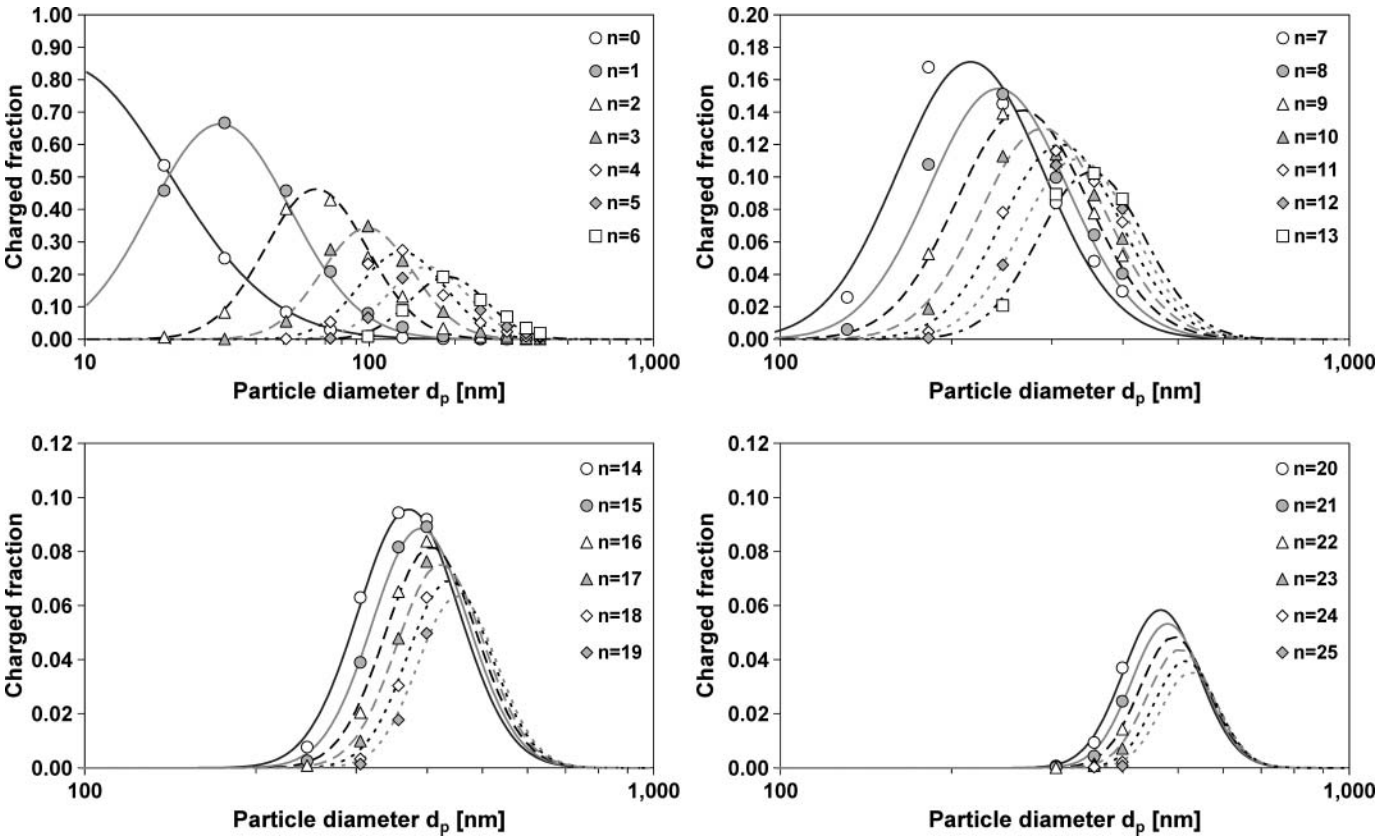

FIG. 7. Charge distributions calculated from Equations (1) and (2), with coefficients in Table 2; symbols indicate measured data.

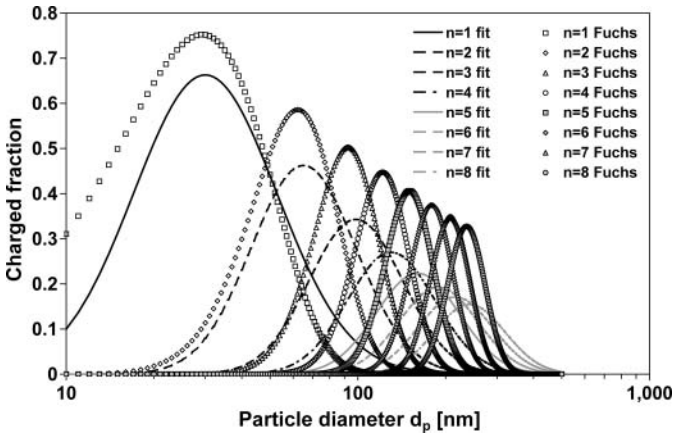

FIG. 8. Charge distributions for 1–8 elementary charges from fitted distributions (according to Equations 1 and 2) and from Fuchs model with an *nt* product of 7×10^{12} s m^{-3}, ion mobility of 1.15×10^{-4} m^2 V^{-1} s^{-1}, and ion mass of 0.13 kg mol^{-1}.

The general agreement for lowly charged particles is acceptable. For higher charge levels, the modal diameters are still in good agreement, whereas the widths of the distributions from Fuchs' model are increasingly smaller than the fitted and hence measured ones. This may be caused by the assumed ideally homogeneous particle and ion distributions in Fuchs' model. In practice, they likely show a spatial distribution in the mixing chamber, because the particles and ions are blown into the chamber from two opposite ends (Figure 1). Close to the injection of the ion jet flow, the ion concentration and particle residence time are high, because particles need to travel further to get to this area. Close to the injection of the aerosol flow, the ion concentration and residence time are low, at least for those particles that take the short direct distance from the particle injection to the chamber outlet. Therefore, as per the *nt* product, particles' encounter in the charger may show a fairly broad distribution depending on the path they take through the charger, which then results in the broader charge distributions, as shown in Figure 8. The comparison of modeled and measured charge distributions shows that Fuchs' model may be used to predict average charge levels, as done by Qi et al. (2009), but cannot deliver accurate charge distributions for the given charger. The mathematical description of the charge distributions cannot hence be done using Fuchs' model but require an empirical approach as described here.

SUMMARY

In this study, the charge distributions of a modified opposed-flow unipolar diffusion charger was measured for 11 monodisperse particle sizes of 19–399 nm and mathematically described. Modifications of the original NSAM charger (Medved et al. 2000) mainly concerned the ease of cleaning and mechanical stability of the corona needle. The charger is intended to be used in a portable size distribution measurement device and hence an accurate mathematical description of the charge fractions is required for implementation in data acquisition and evaluation software. The charger showed average charge levels comparable with the NSAM charger (Jung and Kittelson 2005; Asbach et al. 2011); hence, a similar charger operation can be expected. The charge fractions as a function of particle size could be mathematically fitted to lognormal distributions (Equation 1) with the parameters $A(n)$, which describes the overall probability of a particle to acquire n elementary charges; $B(n)$, which defines the width (geometric standard deviation) of the charge distribution; and $CMD(n)$, which is the count median diameter. The three parameters A, B, and CMD could be fitted to a single equation (Equation 2), which uses five empirical parameter-specific coefficients that were determined for the charger. The set of equations and coefficients can be used to extrapolate the charge level of any particle size at least within the measured size range of approximately 20–400 nm, which is the intended size range of the aforementioned portable aerosol sizer. A comparison of the calculated and measured charge levels showed very high agreement, with regression coefficients $R^2 > 0.96$. Accurate size distribution measurements should hence be possible. The combination of the two equations with the empirical coefficients was implemented in an early version of the data acquisition and evaluation software of the portable aerosol sizer under development. First results are very promising.

The set of equations was only tested for the single unipolar charger presented and is strictly only applicable to this one. However, due to the similarity of the charge distribution shapes from unipolar diffusion chargers (Biskos et al. 2005; Alguacil and Alonso 2006; Qi et al. 2007; Li and Chen 2011), we assume that the equations may even be universally usable for other diffusion chargers with device-specific coefficients K_a through K_e. More investigations will be conducted in the near future to prove this assumption.

REFERENCES

Alguacil, F. J., and Alonso, M. (2006). Multiple Charging of Ultrafine Particles in a Corona Charger. *J. Aerosol Sci.*, 37:875–884.

Asbach, C., Fissan, H., Kaminski, H., Kuhlbusch, T. A. J., Pui, D. Y. H., Shin, H., et al. (2011). A Low Pressure Drop Pre-separator for Elimination of Particles Larger than 450 nm. *Aerosol Air Qual. Res.*, 11:487–496.

Asbach, C., Fissan, H., Stahlmecke, B., Kuhlbusch, T. A. J., and Pui, D. Y. H. (2009). Conceptual Limitations and Extensions of Lung-Deposited Nanoparticle Surface Area Monitor (NSAM). *J. Nanopart. Res.*, 11:101–109.

Azong-Wara, N., Asbach, C., Stahlmecke, B., Fissan, H., Kaminski, H., Plitzko, S., et al. (2009). Optimisation of a Thermophoretic Personal Sampler for Nanoparticle Exposure Studies. *J. Nanopart. Res.*, 11:1611–1624.

Biskos, G., Reavell, K., and Collings, N. (2005). Unipolar Diffusion Charging of Aerosol Particles in the Transition Regime. *J. Aerosol Sci.*, 36:247–265.

Boisdron, Y., and Brock, J. R. (1970). On the Stochastic Nature of the Acquisition of Electrical Charge and Radioactivity by Aerosol Particles. *Atmos. Environ.*, 4:35–50.

Brouwer, D., van Duuren-Stuurman, B., Berges, M., Jankowska, E., Bard, D., and Mark, D. (2009). From Workplace Air Measurement Results Towards Estimates of Exposure? Development of a Strategy to Assess Exposure to Manufactured Nano-Objects. *J. Nanopart. Res.*, 11:1867–1881.

Cena, C. G., Anthony, T. R., and Peters, T. M. (2011). A Personal Nanoparticle Respiratory Deposition (NRD) Sampler. *Environ. Sci. Technol.*, 45:6483–6490.

Chen, D., Pui, D., and Kaufman, S. (1995). Electrospraying of Conduction Liquids for Monodisperse Aerosol Generation in the 4 nm to 1.8 μm Size Range. *J. Aerosol Sci.*, 26:963–977.

Fierz, M., Houle, C., Steigmeier, P., and Burtscher, H. (2011). Design, Calibration, and Field Performance of a Miniature Diffusion Size Classifier. *Aerosol Sci. Technol.*, 45:1–10.

Fissan, H., Neumann, S., Trampe, A., Pui, D. Y. H., and Shin, W. G. (2007): Rationale and Principle of an Instrument Measuring Lung Deposited Nanoparticle Surface Area. *J. Nanopart. Res.*, 9:53–59.

Fuchs, N. (1963). On the Stationary Charge Distribution on Aerosol Particles in Bipolar Ionic Atmosphere. *Geofis. Pura Appl.*, 56:185–193.

Furuuchi, M., Choosong, T., Hata, M., Otani, Y., Tekasakul, P., Takizawa, M., et al. (2010). Development of a Personal Sampler for Evaluating Exposure to Ultrafine Particles. *Aerosol Air Qual. Res.*, 10:30–37.

Hoet, P., Brüske-Hohlfeld, I., and Salata, O. (2004). Nanoparticles – Known and Unknown Health Risks. *J. Nanobiotechnol.*, 2:12

Hoppel, W. (1978). Determination of the Aerosol Size Distribution from the Mobility Distribution of the Charged Fraction of Aerosols. *J. Aerosol Sci.*, 9:41–54.

Jung, H., and Kittelson, D. B. (2005). Characterization of Aerosol Surface Instruments in Transition Regime. *Aerosol Sci. Technol.*, 39:902–911.

Kuhlbusch, T., Asbach, C., Fissan, H., Göhler, D., and Stintz, M. (2011). Nanoparticle Exposure at Nanotechnology Workplaces – A Review. *Particle Fibre Toxicol.*, 8:22.

Li, L., and Chen, D. (2011). Performance Study of a DC-Corona-Based Particle Charger for Charge Conditioning. *J. Aerosol Sci.*, 42:87–99.

Li, L., Chen, D., and Tsai, P. (2009). Use of an Electrical Aerosol Detector (EAD) for Nanoparticle Size Distribution Measurement. *J. Nanopart. Res.*, 11:111–120.

Marra, J., Voetz, M., and Kiesling, K. (2010). Monitor for Detecting and Assessing Exposure to Airborne Nanoparticles. *J. Nanopart. Res.*, 12:21–37.

Maynard, A., and Aitken, R. (2007). Assessing Exposure to Airborne Nanomaterials: Current Abilities and Future Requirements. *Nanotoxicology*, 1:26–41.

Medved, A., Dorman, F., Kaufman, S., and Pocher, A. (2000). New Corona-Based Charger for Aerosol Particles. *J. Aerosol Sci.*, 31:S616–S617.

Methner, M., Hodson, L., Dames, A., and Geraci, C. (2010). Nanoparticle Emission Assessment Technique (NEAT) for the Identification and Measurement of Potential Inhalation Exposure to Engineered Nanomaterials – Part B: Results from 12 Field Studies. *J. Occ. Environ. Hyg.*, 7:163–176.

Methner, M., Hodson, L., and Geraci, C. (2010). Nanoparticle Emission Assessment Technique (NEAT) for the Identification and Measurement of Potential Inhalation Exposure to Engineered Nanomaterials – Part A. *J. Occ. Environ. Hyg.*, 7:127–132.

Nel, A., Xia, T., Mädler, L., and Li, N. (2006). Toxic Potential of Materials at the Nanolevel. *Science*, 311:622–627.

Oberdörster, G. (2000). Toxicology of Ultrafine Particles: In Vivo Studies. *Phil. Trans. R. Soc. A*, 358:2719–2740.

Oberdörster, G., Oberdörster, E., and Oberdörster, J. (2007). Concepts of Nanoparticle Dose Metric and Response Metric. *Environ. Health Persp.*, 115:A290–A294.

Park, D., Kim, Y-H., Lee, S-G., Kim, C., Hwang, J., and Kim, Y-J. (2010). Development and Performance Test of a Micromachined Unipolar Charger for Measurements of Submicron Aerosol Particles Having a Log-Normal Size Distribution. *J. Aerosol Sci.*, 41:490–500.

Poland, C. A., Duffin, R., Kinloch, I., Maynard, A., Wallace, W. A. H., Seaton, A., et al. (2008). Carbon Nanotubes Introduced into the Abdominal Cavity of Mice Show Asbestos-Like Pathogenicity in a Pilot Study. *Nature Nanotechnol.*, 3:423–428.

Qi, C., Asbach, C., Shin, W., Fissan, H., and Pui, D. Y. H. (2009). The Effect of Particle Pre-Existing Charge on Unipolar Charging and Its Implication on Electrical Aerosol Measurements. *Aerosol Sci. Technol.*, 43:232–240.

Qi, C., Chen, D., and Greenberg, P. (2008). Performance Study of a Unipolar Aerosol Mini-Charger for a Personal Nanoparticle Sizer. *J. Aerosol Sci.*, 39:450–459.

Qi, C., Chen, D., and Pui, D. Y. H. (2007). Experimental Study of a New Corona-Based Unipolar Aerosol Charger. *J. Aerosol Sci.*, 38:775–792.

Schulte, P., Geraci, C., Zumwalde, R., Hoover, M., and Kuempel, E. (2008). Occupational Risk Management of Engineered Nanoparticles. *J. Occ. Environ. Hyg.*, 5:239–249.

Shin, W., Pui, D., Fissan, H., Neumann, S., and Trampe, A. (2007). Calibration and Numerical Simulation of Nanoparticle Surface Area Monitor (TSI Model 3550 NSAM). *J. Nanopart. Res.*, 9:61–69.

VCI – German Chemical Industry Association. (2011) Exposure Measurement and Assessment of Nanoscale Aerosols, available from https://www.vci.de/Services/Leitfaeden/Seiten/Aerosols-Released-from-Engineered-Nanomaterials-in-Workplace-Operations.aspx#

Wiedensohler, A. (1988). An Approximation of the Bipolar Charge Distribution for Particles in the Submicron Size Range. *J. Aerosol Sci.*, 19:387–389.

Wittmaack, K. (2007). In Search of the Most Relevant Parameter for Quantifying Lung Inflammatory Response to Nanoparticle Exposure: Particle Number, Surface Area, or What? *Environ. Health Persp.*, 115:187–194.